Ionic conductivity in multiply substituted ceria-based electrolytes

Alice V. Coles-Aldridge, Richard T. Baker*

EaStChem, School of Chemistry, University of St. Andrews

North Haugh, St Andrews, Fife, KY16 9ST, United Kingdom

*Corresponding author. Tel.: +44 1334 463899; Fax: +44 1334 463808; E-mail: rtb5@st-andrews.ac.uk

Abstract

Cerias, appropriately doped with trivalent rare earth ions, have high oxide ion conductivity and are attractive SOFC (solid oxide fuel cell) electrolytes. Here, seven compositions of $Ce_{0.8}Sm_xGd_yNd_zO_{1.9}$ (where x, y and z = 0.2, 0.1, 0.0667 or 0 and $x + y + z$ = 0.2) are synthesised using a low temperature method in order to determine the effect of multiple doping on microstructure and conductivity. Analysis using scanning and transmission electron microscopy, inductively coupled plasma mass spectrometry, X-ray diffraction and impedance spectroscopy is carried out. Crystallite sizes are determined in the powders and relative densities and grain size distributions were obtained in sintered pellets. Total, bulk and grain boundary conductivities are obtained using impedance spectroscopy and corresponding activation energies and enthalpies of ion migration and defect association are calculated. The highest total conductivity observed at 600 °C is 1.80 Sm^{-1} for $Ce_{0.8}Sm_{0.1}Gd_{0.1}O_{1.9}$ and an enhancement effect on conductivity for this combination of co-dopants between 300 °C and 700 °C relative to the singly doped compounds - $Ce_{0.8}Sm_{0.2}O_{1.9}$ and $Ce_{0.8}Gd_{0.2}O_{1.9}$ - is seen. This has interesting implications for application as SOFC electrolytes, especially at intermediate temperatures.

1. Introduction

The clean and efficient generation of electricity is a pressing global challenge. Fuel cells convert chemical energy from a gaseous fuel and oxidant directly into electrical work and SOFCs in particular exhibit high efficiencies, low pollutant emissions, fuel flexibility and suitability for Combined Heat and Power applications.[1] Therefore, SOFCs are likely to play an important part in energy conversion in the near future and are being developed for commercial applications ranging from domestic units to small power stations.[2],[3],[4] So far, widespread use of SOFCs has been inhibited by their high operating temperatures of typically 800 to 1000 °C.[5] A move to Intermediate temperature (IT)-SOFCs, which operate between 500 and 750 °C – is desirable in order to widen the range of structural and functional materials that can be used, and reduce energy usage, electrode sintering, interfacial diffusion between electrolyte and electrodes and thermal stress.[6],[7] However, the lower ionic conductivity of the electrolyte at these lower temperatures can limit the performance of IT-SOFCs. Therefore, optimising electrolyte design to increase conductivity to acceptable levels at these temperatures becomes central.

Electrolytes based on ceria demonstrate higher oxide ion conductivity at IT than YSZ (yttria-stabilised zirconia), the most commonly used electrolyte in SOFCs. A structure containing a large number of interconnected, equivalent and partially occupied sites for the oxide ion is required for high intrinsic (or 'bulk') ionic conductivity. This is achieved by aliovalent doping of the material - the partial substitution of Ce^{4+} ions by tri- or divalent cations in order to create oxygen vacancies to maintain charge neutrality.[8] The relatively facile migration of these vacancies in the cubic anionic sublattice at elevated temperatures then gives rise to fast ionic transport through the electrolyte.[9]

Reports have shown that ceria doped with certain trivalent rare earth ions gives higher bulk ionic conductivity than those doped with other elements.[10] The concept of matching the size of the trivalent dopant ion to that of Ce^{4+} (0.97 Å) in order to minimise both strain and activation energy for oxygen vacancy diffusion, E_a, is an important consideration.[11],[12],[13] In this approach, to optimise bulk ionic conductivity, the repulsive elastic (related to dopant radius) and attractive electronic components of the interaction between vacancies and dopant ions should balance. According to research by Andersson *et al* using *ab initio* methods, this is the case for a hypothetical atomic number between 61 (Pm) and 62 (Sm). Pm is radioactive, so a combination of alternative lanthanide dopant ions with

an average atomic number between 61 and 62 was proposed to optimise bulk ionic conductivity in electrolytes based on ceria.[14] This hypothesis was investigated experimentally in work by Omar et al in which Sm^{3+} and Nd^{3+} were selected to form electrolytes of composition, $Sm_{x/2}Nd_{x/2}Ce_{1-x}O_{2-\delta}$ (with x=0.01 - 0.2), in which the average atomic number of the dopants was therefore 61. The authors interpreted the adherence of this compositional series to a linear relationship between **x** and unit cell parameter, **a** (Vegard's law) as an indication that less short-range ordering of oxygen vacancies and dopant cations occurred in these materials than in singly-doped materials, such as the series, $Nd_xCe_{1-x}O_{2-\delta}$, reported by Stephens and Kilner which displayed a second-order dependence.[15] This lack of defect ordering was proposed to result from a similarity in energy of the sites available to host oxygen ion vacancies which was given in turn as the reason for improved ionic conductivity. At 550 °C, $Sm_{0.05}Nd_{0.05}Ce_{0.10}O_{2-\delta}$ was found to have a higher bulk ionic conductivity than the widely used, analogous composition, $Gd_{0.10}Ce_{0.90}O_{2-\delta}$, so supporting the hypothesis of Andersson described above.[16]

The ideal average atomic number between 61 and 62 also corresponds to a critical dopant ionic radius (r_C). Omar et al ensured that the average dopant ionic radius of the synthesised $Lu_xNd_yCe_{1-x-y}O_{2-y}$ matched r_C for all compositions in order to investigate the effect of elastic strain in the lattice on bulk ionic conductivity.[17] It was found that the elastic strain in the doubly doped system was negligible compared to the parent singly doped systems and that the bulk ionic conductivity was higher for the doubly doped system than for the corresponding singly doped systems. Therefore, it was concluded that co-doping based on r_C can lead to increased conductivity for ceria electrolytes. In a later paper, however, the same authors concluded that r_C alone was insufficient to fully explain the conductivity of doped cerias.[18]

Wang and co-workers observed a higher total conductivity for $Ce_{0.85}Gd_{0.15-y}Sm_yO_{1.925}$ (0.05 ≤ y ≤ 0.1) than for $Ce_{0.85}Gd_{0.15}O_{1.925}$ or $Ce_{0.85}Sm_{0.15}O_{1.925}$ between 500 and 700 °C .[19] This was attributed to suppression of the ordering of oxygen vacancies and hence a lower activation energy for the co-doped ceria than for the singly doped ceria. Anirban and co-workers observed that ceria co-doped with Gd^{3+} and Nd^{3+} exhibited a slight increase in bulk conductivity and a more significant increase in grain boundary conductivity compared to the singly doped specimens with the same dopant concentration with the effect of co-doping increasing at 600 °C and above.[20] Liu and co-workers found that, of all the Sm^{3+} and Nd^{3+} co-doped and singly doped compositions investigated, the highest total ionic conductivity was observed for $Ce_{0.8}Sm_{0.1}Nd_{0.1}O_{1.9}$.[21] These studies show that co-doping can have beneficial effects on the conductivity of ceria-based electrolytes. However, computational work by Burbano and co-workers

predicted that the bulk ionic conductivity of co-doped systems lies within the range spanned by the singly doped materials between 600 and 1000 °C.[22] Whether the co-doping of ceria has a synergistic, detrimental or averaging effect on ionic conductivity will determine which compositions emerge as the most promising ceria-based electrolytes and whether these can be successfully applied in IT-SOFCs.

There is no overall consensus on the best dopant or combination of dopants for ceria-based electrolytes. Therefore, in this work, seven nanopowders with the composition $Ce_{0.8}Sm_xGd_yNd_zO_{1.9}$ where x, y and z = 0.2, 0.1, 0.667 or 0 and $x + y + z$ = 0.2 were synthesised. The chemical composition, powder nanostructure and crystal phase of these products were studied as were the microstructure and total, bulk and grain boundary ionic conductivities of the dense electrolyte pellets prepared from these powders. The results and analyses were cross-compared to gain insight into the parameters determining favourable performance in these materials.

2. Experimental

Seven compositions of $Ce_{0.8}Sm_xGd_yNd_zO_{1.9}$ were prepared where x, y and z = 0.2, 0.1, 0.667 or 0 and $x + y + z$ = 0.2 (see Table 1). 0.1 mol dm^{-3} solutions were made by dissolving stoichiometric amounts of metal nitrate hexahydrates, $Ce(NO_3)_3.6H_2O$ (Acros Organics, 99.5 %), $Sm(NO_3)_3.6H_2O$ (Acros Organics, 99.9 %), $Gd(NO_3)_3.6H_2O$ (Acros Ogranics, 99.9 %) and $Nd(NO_3)_3.6H_2O$ (Aldrich, 99.9%) separately in deionised water. They were stirred for 3 h to homogenise before being combined. A 0.2 mol dm^{-3} citric acid solution was made by dissolving anhydrous citric acid (Alfa Aesar, 99.5 %) in deionised water and stirring for 3 h to homogenise prior to being added to the metal cation solution in the ratio of one mole of total metal cations to two moles of citrate. The resulting solution was stirred for 12 h to achieve homogenisation, heated to 80 °C and maintained under stirring for 24 h. Evolution of steam and gas resulted in a gel and finally a solid yellow foam. Thermal decomposition of the foam was carried out in a muffle furnace at 250 °C for 2 h and the resulting powder was calcined in a muffle furnace at 500 °C for 2 h. Heating and cooling rates were 2.5 °C min^{-1} and 5 °C min^{-1} respectively. The powders were dry ground for 1 h at 400 rpm in a planetary ball mill (Fritsch Pulverisette 7)[23] using Nylon jars and 10 mm diameter zirconia balls as the grinding medium and a powder to ball weight ratio of 1:10. It was necessary to suspend the ball milling process every 15 minutes in order to displace the powder from the walls of the jar. The seven resulting nanopowder compositions underwent detailed characterisation.
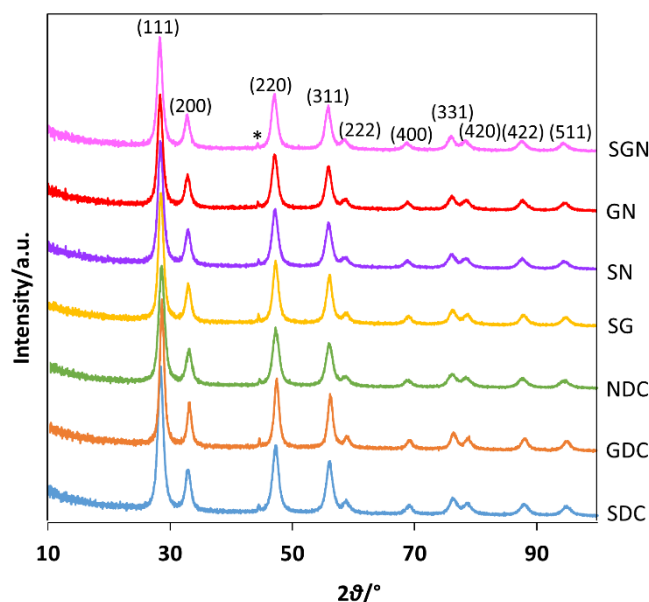
Figure 1. XRD patterns for powder samples of $Ce_{0.8}Sm_xGd_yNd_zO_{1.9}$ for all compositions. *Small peak at about 45° is due to the sample holder (main peak of Fe).

To make sintered electrolyte pellets, the powders were uniaxially pressed at 200 MPa in a 25 mm (for impedance spectroscopy) or 10 mm (for examination using SEM, scanning electron microsopy) diameter, cylindrical stainless steel dye. The pellets were sintered at 1450 °C for 4 h with a heating rate of 2 °C min^{-1} and a cooling rate of 4 °C min^{-1} in accordance with the method used previously for the synthesis of samarium doped ceria (SDC).[24] The sintered pellets were polished using 600 and 1200 grade silicon carbide paper and 6 μm diamond paste (and 3 μm diamond paste for the SEM pellets) resulting in a mirror finish.

XRD (X-ray diffraction) analysis of the samples was carried out using a PANalytical Empyrean diffractometer with Cu $K\alpha_1$ monochromatic radiation. The external standard used was high-grade silicon powder which allowed correction for instrumental broadening. Data were acquired at room temperature by scanning 2ϑ from 10° to 100° with a step size of 0.017 ° and a step time of 0.95 s. The XRD patterns were fitted using Rietveld operations in the High Score Plus programme.

The nanopowders were dissolved in concentrated nitric acid in Teflon-lined autoclaves at 160 °C for 8 h for analysis by ICP-MS (inductively coupled plasma- mass spectrometry) using an Agilent 7500ce with Ar gas flows of 0.82 L min^{-1} (carrier) and 0.2 L min^{-1} (makeup). Sample solutions were taken into the nebuliser at a rate of approximately 1.0 mL min^{-1}. Three runs for each sample were carried out and each mass was analysed in fully quantitative mode (three points per unit mass). ^{140}Ce, ^{157}Gd, ^{146}Nd and ^{147}Sm were analysed in no gas mode. Calibration standards were prepared

using single element 1000 mg L^{-1} stock solutions for Ce, Gd, Nd and Sm (Qmx), diluted with 2% HNO_3 v/v (Aristar grade, Merck).

SEM images of the pellets were obtained using a JEOL JSM-6700F instrument equipped with a field emission gun at 5.0 kV and were used to carry out statistical grain area analyses on each sample where the areas of many grains (> 400) were measured using ImageJ software. For SEM polished pellets were thermally etched at 1400 °C, employing a dwell time of 1 min. and identical ramp rates to those used in the sintering process. Samples were gold-coated to reduce charging. A JEOL JEM-2011 instrument was used to acquire TEM (transmission electron microscope) images for crystallite size analysis. Samples were prepared by submerging 3 mm holey carbon Cu grids in an ultrasonicated dispersion of the powder in acetone. The Cu grids were dried overnight.

The dimensions and masses of the sintered pellets were used to calculate their densities. Relative density values were obtained by dividing these density values by the corresponding theoretical density, ρ_{XRD}, calculated using Equation 1 from the crystallographic information obtained by XRD, where M_i is the atomic mass of element i; x, y and z = 0.2, 0.1, 0.667 or 0 (and $x + y + z = 0.2$) and u is the atomic mass unit and V is the unit cell volume.

$$\rho_{XRD} = \frac{u \times (((0.8 \times M_{Ce}) + (x \times M_{Sm}) + (y \times M_{Gd}) + (z \times M_{Nd})) \times 4) + ((0.9 \times M_O) \times 8)}{V} \qquad (1)$$

Two-electrode impedance spectroscopy was performed on the electrolyte pellets using a Solartron 1260 FRA instrument. Electrodes were deposited by screen-printing Pt ink (inorganic-free, Engelhardt) on each side of the pellets and firing at 1000 °C for 1 h with heating and cooling rates of 2 °C min^{-1}. The resulting cells were placed in a tube furnace and impedance measurements were carried out under flowing pre-dried, synthetic air (50 ml min^{-1}) at intervals of 50 °C between 150 - 900 °C, during both heating and cooling ramps. An A.C. voltage of 100 mV (250 °C – 900 °C) or 500 mV (150 °C – 200 °C) was applied and the frequency was swept from 10 MHz to 1 Hz. At each measurement temperature, multiple spectra were recorded until there were no variations between them. ZView software (Scribner Associates, Inc.) was used to analyse the impedance spectra.

3. Results and Discussion

3.1. Powder Characterisation

After calcination, the products consisted of voluminous fragile, papery structures which yielded very, pale yellow nanopowders after milling. XRD patterns of the seven $Ce_{0.8}Sm_xGd_yNd_zO_{1.9}$ nanopowders are given in Figure 1. All peaks could be assigned to the cubic fluorite *Fm-3m* crystal structure. There was no evidence of any other phases indicating that the powders were homogeneous and that the dopants were soluble in the cerium oxide lattice. Figure 2 presents lattice parameter, crystallite size and relative density as a function of average cation ionic radius. The lattice parameter (*a*, determined by Rietveld refinement of the XRD data) increased from 5.4244 Å ($Ce_{0.8}Gd_{0.2}O_{1.9}$) to 5.4446 Å ($Ce_{0.8}Nd_{0.2}O_{1.9}$). This showed a strong linear dependence when plotted against the average ionic radii of the trivalent dopant ions for each composition (Figure 2a) indicating that Vegard's Law was obeyed in these materials, in spite of the presence of different cation combinations.[25] Table 1 summarises the lattice parameters and the average crystallite diameters (D_{XRD}) of the seven powders obtained from the XRD data. Crystallite diameter was calculated from the extent of line broadening of the principal (111) diffraction peak using the Scherrer equation.[26] It decreased as the average ionic radius of the dopants increased, from 93 Å for $Ce_{0.8}Gd_{0.2}O_{1.9}$ to 55 Å for $Ce_{0.8}Nd_{0.2}O_{1.9}$ (Figure 2b).

These values are comparable to those from previous work using the same synthesis method.[24] TEM images of each of the seven samples were used to calculate the average diameter of the individual crystallites, D_{TEM}, (see Table 1, Figure 2b and Figure S1 in Electronic Supplementary Information (ESI)). This showed a similar trend to D_{XRD}, although at higher values. This difference between the D_{XRD} and the D_{TEM} values is attributed to the difficulty of reliably identifying very small nanocrystals in the TEM, especially since the crystallites were arranged in loosely agglomerated clusters – and therefore overlapping in the images - for all compositions. Individual particles were seen by high resolution TEM to have excellent crystallinity with no evidence of crystallites containing multiple nanodomains. The decreasing trend in crystallite size with increasing average ionic radius may be related to decreasing ionic diffusion rates as cation size increased.
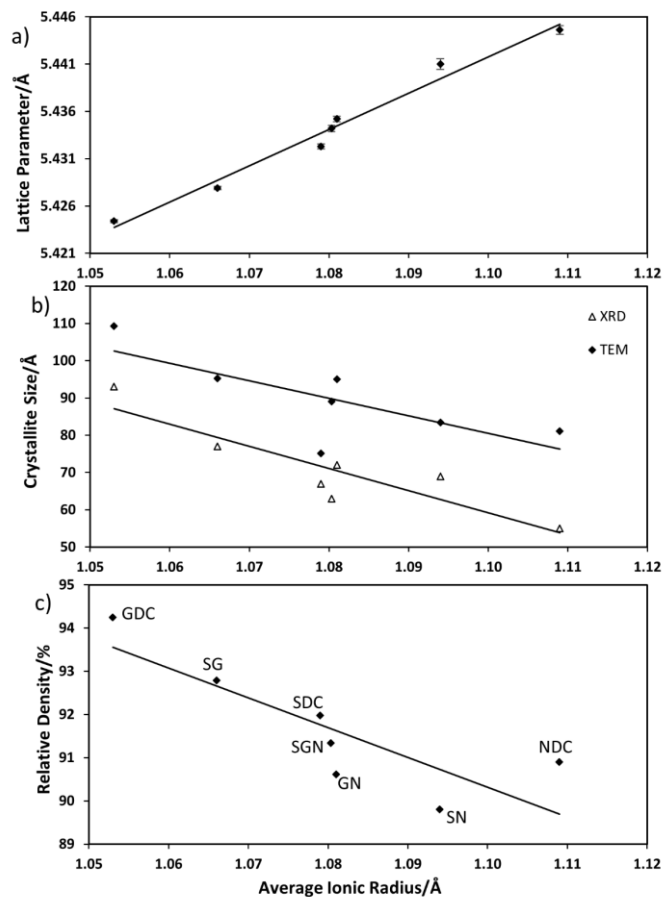
Figure 2. Dependence on average ionic radius of dopant ions in $Ce_{0.8}Sm_xGd_yNd_zO_{1.9}$ of a) lattice parameter obtained from powder XRD; b) average crystallite size calculated from powder XRD data and TEM images; c) relative density of pellets sintered at 1450°C for 4h. The best fit lines are added as guides to the eye.

ICP-MS was used for elemental analysis and the values are reported in Table 2 as cation % with associated errors (one standard deviation). No major impurities were identified in any of the compositions. However, there are discrepancies between the nominal stoichiometries and the ICP-MS results. Although the dopant concentrations are slightly higher than expected, the total dopant concentration is close to constant for all samples meaning the oxygen vacancy concentration (which is directly determined by the dopant concentration) is expected to be near-identical in each case. Therefore, comparisons between samples can be made based on the different individual dopant concentrations and identities. Unexpected Sm, Gd or Nd in a sample is likely to have been introduced from the starting nitrates (which were also analysed using ICP-MS). In the most important case, the remaining 0.5 % in the 99.5 % pure cerium nitrate hexahydrate was found to primarily consist of a gadolinium compound. This led to the slight excesses seen for this particular dopant.

3.2 Pellet Characterisation

Pellets were sintered at 1450 °C for 4 h because this is close to the regime found to give maximum conductivity in SDC in previous work by Kosinski and Baker which also used the citrate-nitrate synthesis method.[24] The relative densities ranged from 89.8 % for $Ce_{0.8}Sm_{0.1}Nd_{0.1}O_{1.9}$ to 94.3 % for $Ce_{0.8}Gd_{0.2}O_{1.9}$. There is a general decrease in relative density with increasing average ionic radius of the dopant lanthanides comprising the sample (Figure 2c). The rate of cation diffusion at the high temperatures of synthesis and sintering is likely to decrease as average cation size increases. This may explain the similar decreasing trend in crystallite size (see above). Both these trends - of decreasing crystallite size and decreasing cation diffusion rate with increasing cation size – may contribute to limit the degree of sintering and cause the corresponding decrease in relative density..

Figure 3 shows SEM images of the fired samples after polishing and thermal etching. Interlocking grains of typical, approximately hexagonal shape were observed. Grain areas are presented as normalised distribution histograms next to the corresponding images in Figure 3. These exhibit an approximately log-normal distribution of grain sizes with similar modal grain areas for each sample showing that grain growth was normal for all samples.[24] Average grain sizes were not found to correlate with crystallite size, relative density nor the average ionic radius of the trivalent dopants (Figure 4) and grain areas ranged from 0.249 μm^2 for $Ce_{0.8}Gd_{0.2}O_{1.9}$ to 0.414 μm^2 for $Ce_{0.8}Sm_{0.1}Gd_{0.1}O_{1.9}$. This contrasts with the trends in powder crystallite diameter and relative density of the sintered pellet, both of which showed a general decrease with increasing average ionic radius of the dopants. In the SEM images all samples show a small amount of porosity, accounting for the lower than expected relative density of all samples. Grain growth could have been limited by these pores pinning the grain boundaries. This differs from the results of Kosinski and Baker where sintering conditions of 1450 °C for 4 h produced samples with lower porosity and larger grains.[24] There is a small possibility that the higher porosity than expected for these samples is due to oversintering. This phenomenon was reported by Liu *et al*[21] for the composition $Ce_{0.8}Sm_{0.1}Nd_{0.1}O_{1.9}$ when sintered for 5 h at 1500°C and (more markedly) 1600°C and proposed by Kosinski and Baker[24] for sintering conditions of 1450 °C for 6 h. However, it should be noted that the grains were larger in these studies than in the present contribution.
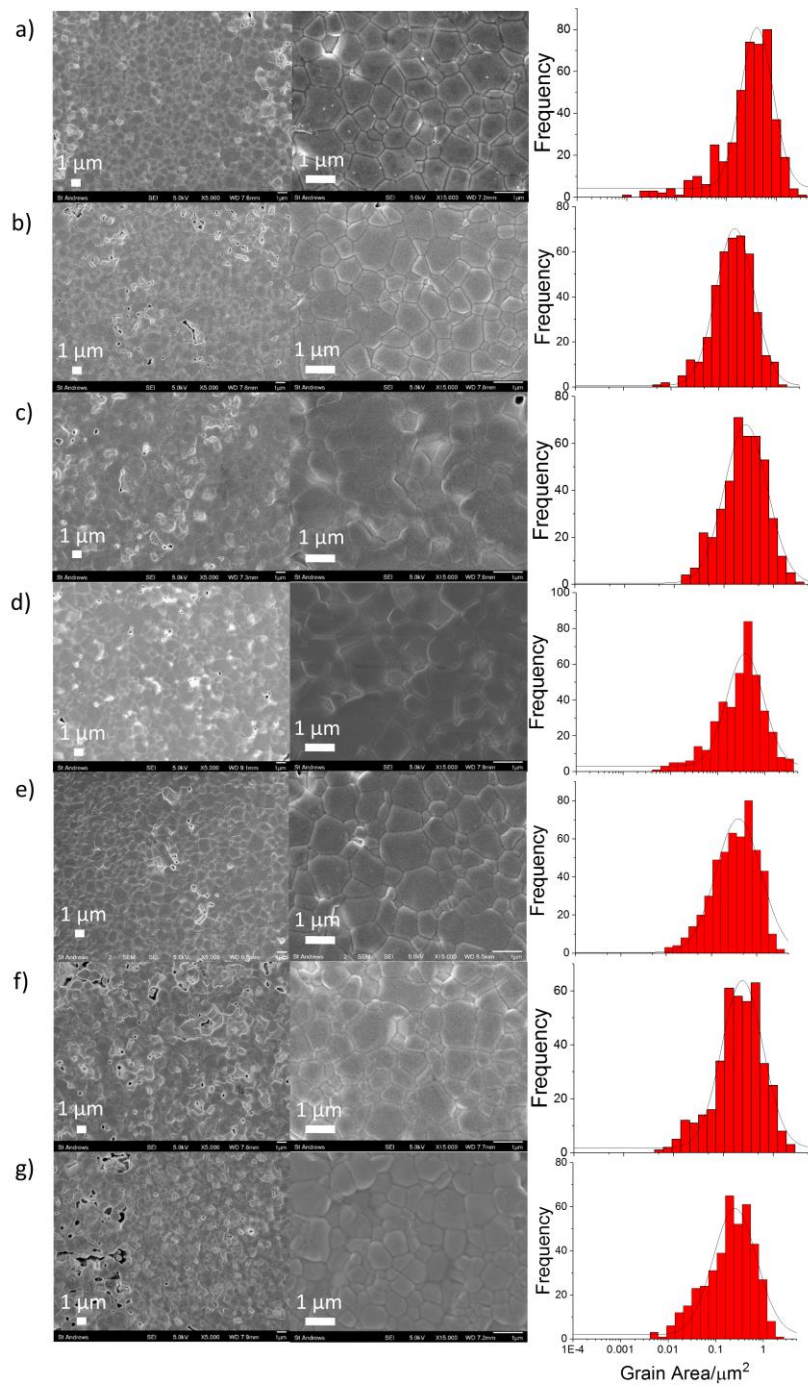
Figure 3. SEM images at intermediate and high magnification alongside log histograms showing the grain area distributions for samples sintered at 1450°C for 4h: a) SDC, b) GDC, c) NDC, d), SG, e) SN, f) GN and g) SGN.
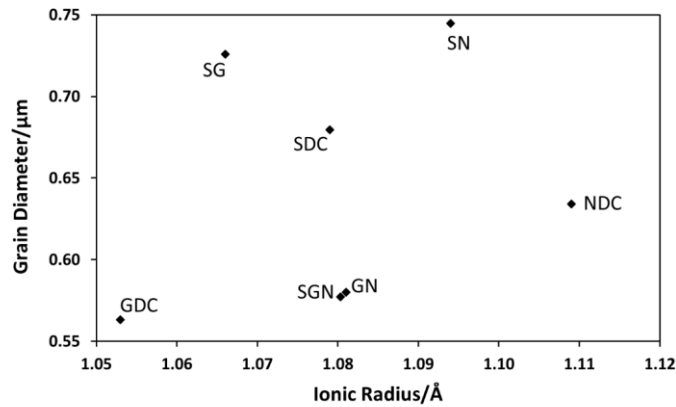
Figure 4. Average grain diameter (calculated from grain areas with the assumption that grain cross-sections are circular) as a function of average ionic radius of dopant ions for $Ce_{0.8}Sm_xGd_yNd_zO_{1.9}$ samples sintered at 1450°C for 4 h.

3.3 Electrical Properties

Electronic conductivity was considered to be negligible under the oxidising conditions used in this work. Even at the highest temperature of 900 °C used to measure impedance where the reduction of ceria is most prevalent, the contribution to the total conductivity due to electronic conductivity is less than 1 %.[27],[28],[29],[30]

Impedance spectra are presented as Nyquist plots in Figure 5 for all seven compositions. At low temperatures (150 – 400 °C) two arcs are visible in the spectra. The higher frequency arc was assigned to bulk (intra-granular) ionic conduction and the smaller arc at lower frequency to ionic conduction across the grain boundaries (inter-granular). Total, bulk and grain boundary conductivities were calculated from the resistances acquired from the impedance spectra, the area of the Pt electrodes and the thickness of the electrolyte pellets. At intermediate (450 – 550 °C) and high (600 – 900 °C) temperatures, the bulk arc was progressively obscured by the inductance of the apparatus and shifted above the operating frequency window of the spectrometer. Therefore, separate bulk and grain boundary conductivities were obtained from the spectra only for the lower temperatures, while total conductivities (bulk plus grain boundary) are given for all temperatures, since these could be obtained from the intercept with the Z' axis in the absence of the bulk arc. Values of capacitance were extracted from the fits to the Nqiust plots. At 300 °C values were very similar - at $0.95\text{-}1.1 \times 10^{-10}$ F – for the bulk arc and $2.1 – 4.9 \times 10^{-9}$ F for the grain boundary arc. Capacitances of around 10^{-6} F extracted from the main arc observed at high temperatures are characteristic of charge transfer
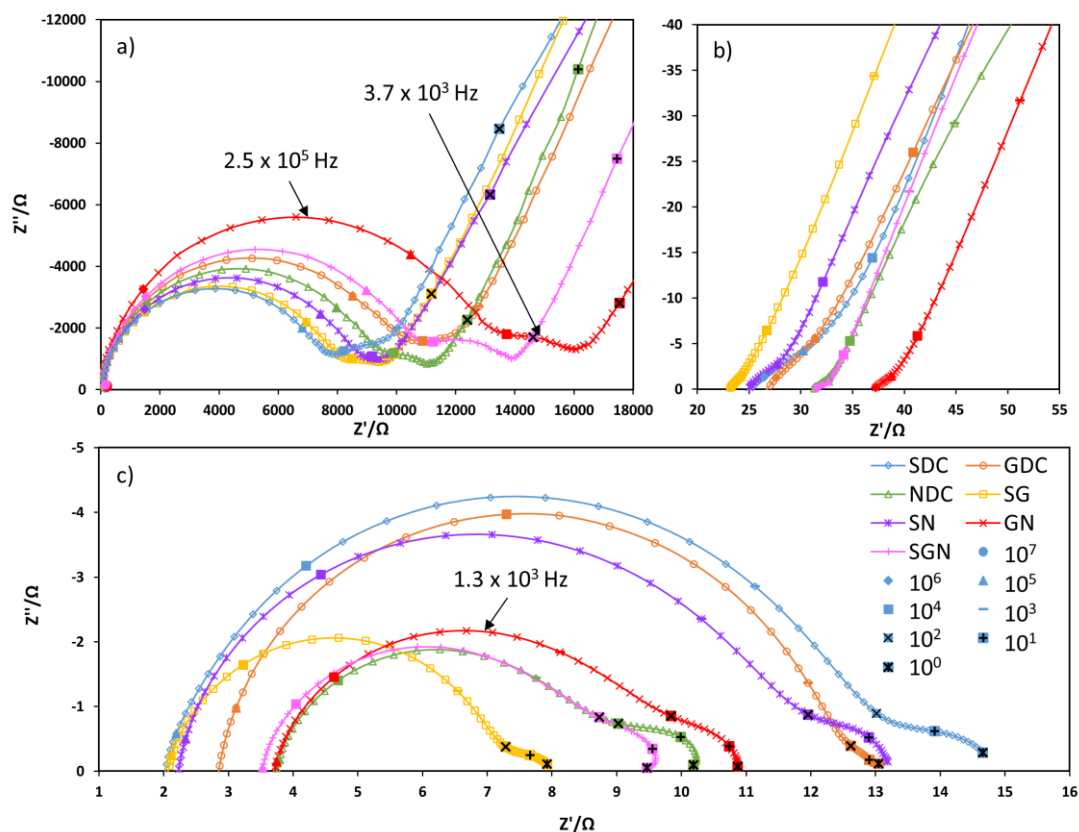
11

Figure 5. Nyquist plots for SDC, GDC, NDC, SG, SN, GN and SGN at a) 250°C, b) 500°C and c) 750°C. Different symbols represent the change in frequency decade, the key for which is inset in panel (c).

processes at the electrode-electrolyte interface.[31] The smaller, low frequency arc at 750 °C can be assigned to electrode processes.

3.3.1 Conductivities

Figure 6 displays Arrhenius-type plots of the total, bulk and grain boundary conductivities for the SG sample, by way of example (plots for all seven samples are available as Figure S2 in the ESI). Grain boundary conductivity was much higher (by at least a factor of 4.5) than bulk conductivity for all of the compositions studied. Because of this, total conductivity was determined essentially by the bulk conductivity. This indicates that the materials synthesised in this work had low levels of impurities since these tend to accumulate at grain boundaries and have a particularly strong negative effect on grain boundary conductivity. Indeed, Si – the most problematic impurity in SOFC electrolyte materials – was found to be below the detection limits of 25 ppm in ICP-MS in the materials used in this study and below 10 ppm in XPS for multiply-doped cerias prepared in the same way (T. Sherwood, R.T. Baker, unpublished work).
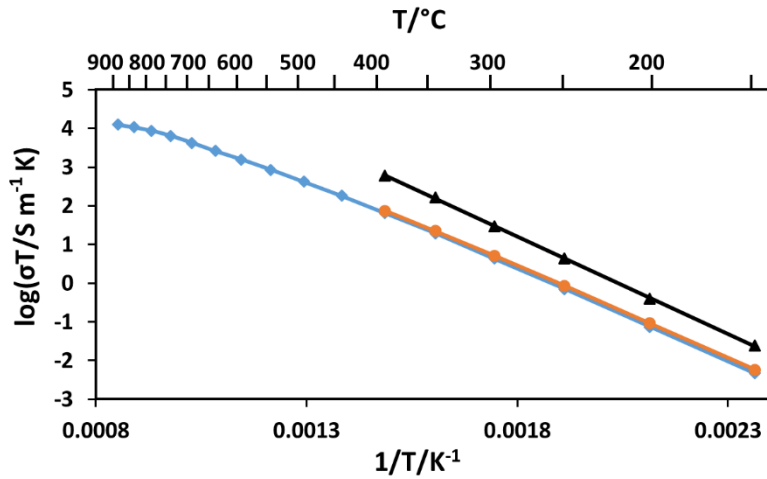
Figure 6. Arrhenius plots of total (♦), bulk (●) and grain boundary (▲) conductivity for SG.

In the log plots presented in Figure 7 it is possible to compare the total, bulk and grain boundary conductivities for all samples over a wide range of temperatures. Variations in total conductivity are the most significant. Grain boundary conductivity is generally very high – attributed to the high purity of these materials – and this leads to the close dependence seen of total conductivity on bulk conductivity. In all plots, a trough in conductivity occurs for the two samples containing both Gd and Nd dopants, SGN and GN. It may be significant that these dopants occupy the two extremes of ionic radius of the dopants studied here. In Figure 7(b), the bulk conductivity of SG overtakes that of SDC, to become the most conductive, as temperature increases. In Figure 7(a), this trend continues for total conductivity until SDC becomes dominant again at 800°C.

In order to study more closely the differences between compositions, normalised bulk (σ_b) and grain boundary (σ_{gb}) conductivities are plotted against temperature for all samples in Figure 8(a) and (b) and normalised total conductivity (σ_t) is plotted in the same way in Figure 8(c). The normalisations were carried out by dividing each conductivity value by the corresponding value for the SDC sample at the same measurement temperature.

Bulk conductivity was highest for SDC between 150 °C and 250 °C and for SG from 300 °C to 400 °C and was lowest for GDC at 150 °C and for GN between 200 °C and 400 °C. The presence of Gd appears to cause normalised σ_b to increase with temperature with respect to SDC, while Nd results in a decrease and where both are present the plot is roughly flat.
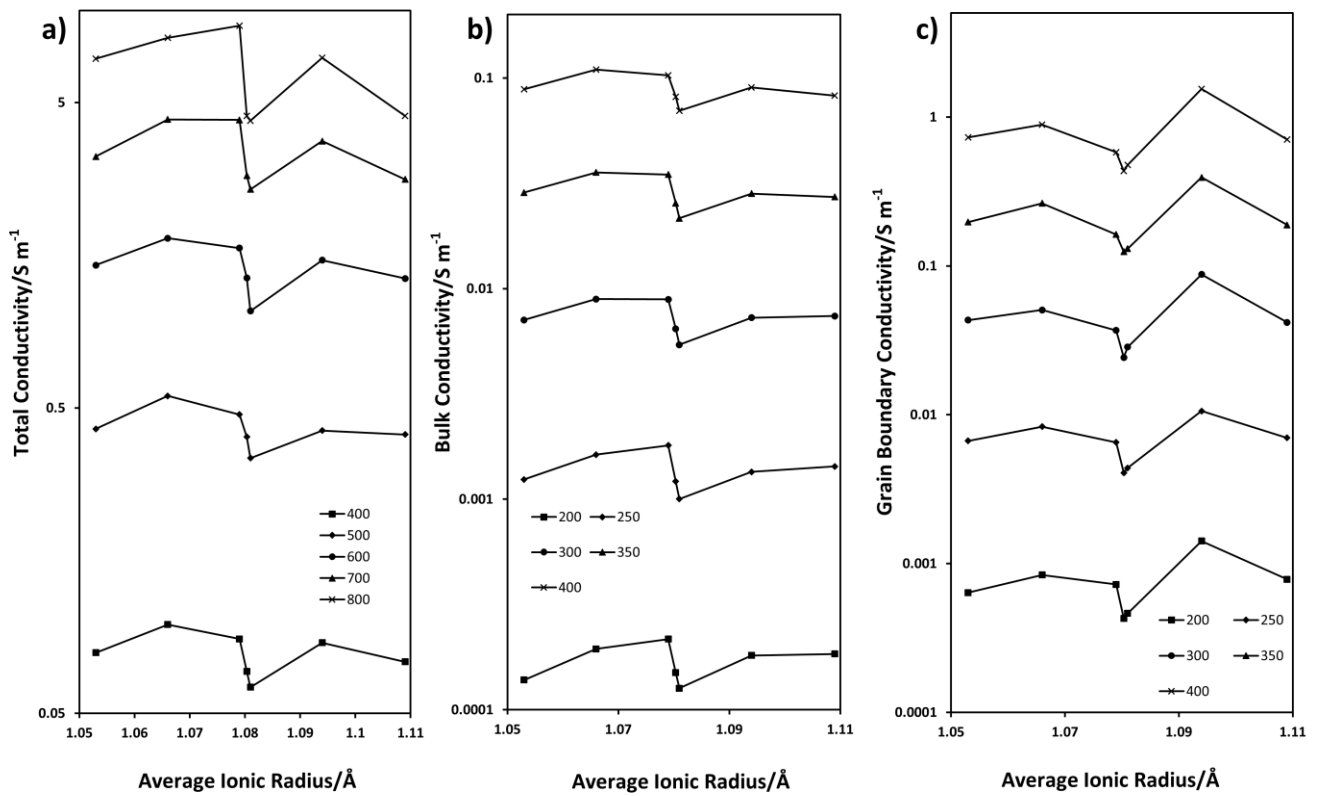
Figure 7. Log plots of (a) total, (b) bulk and (c) grain boundary conductivity as a function of average ionic radius for all samples.

In Figure 8(b), grain boundary conductivity was highest for SN at all temperatures for which σ_{gb} could be calculated, from 150 °C to 400 °C. It was lowest for GDC at 150 °C and SGN from 200 °C to 400 °C. The different sample compositions were in a very similar order to that seen for bulk conductivity. This suggests that intrinsic (bulk) conductivity is an important factor in σ_{gb}. The main differences were that SN rose up the order, and SDC and SGN fell. These changes cannot be simply accounted for by considering the grain size and density of the samples. The relatively small size of the grain boundary arcs (and so the errors in fitting them) and the small variations seen in relative density and in grain diameter across the sample series make it difficult to interpret the differences in σ_{gb} values in terms of microstructural parameters. Also, the different chemical compositions are likely to have some direct effect on the properties of the grain boundaries.

The total conductivity of 1.67 S m^{-1} for SDC at 600 °C is very similar to the 1.81 S m^{-1} obtained by Kosinski and Baker for $Ce_{0.8}Sm_{0.2}O_{1.9}$ at the same temperature although in this case a sintering time of 6 h was used.[24] However, it was higher than those of Balazs and co-workers of 1.2 S m^{-1} at 600 °C for $Ce_{0.2}Sm_{0.8}O_{1.9}$ and of Zhan and co-workers for the same composition synthesised *via* traditional ceramic routes.[32],[33] These lower conductivities are mostly due to
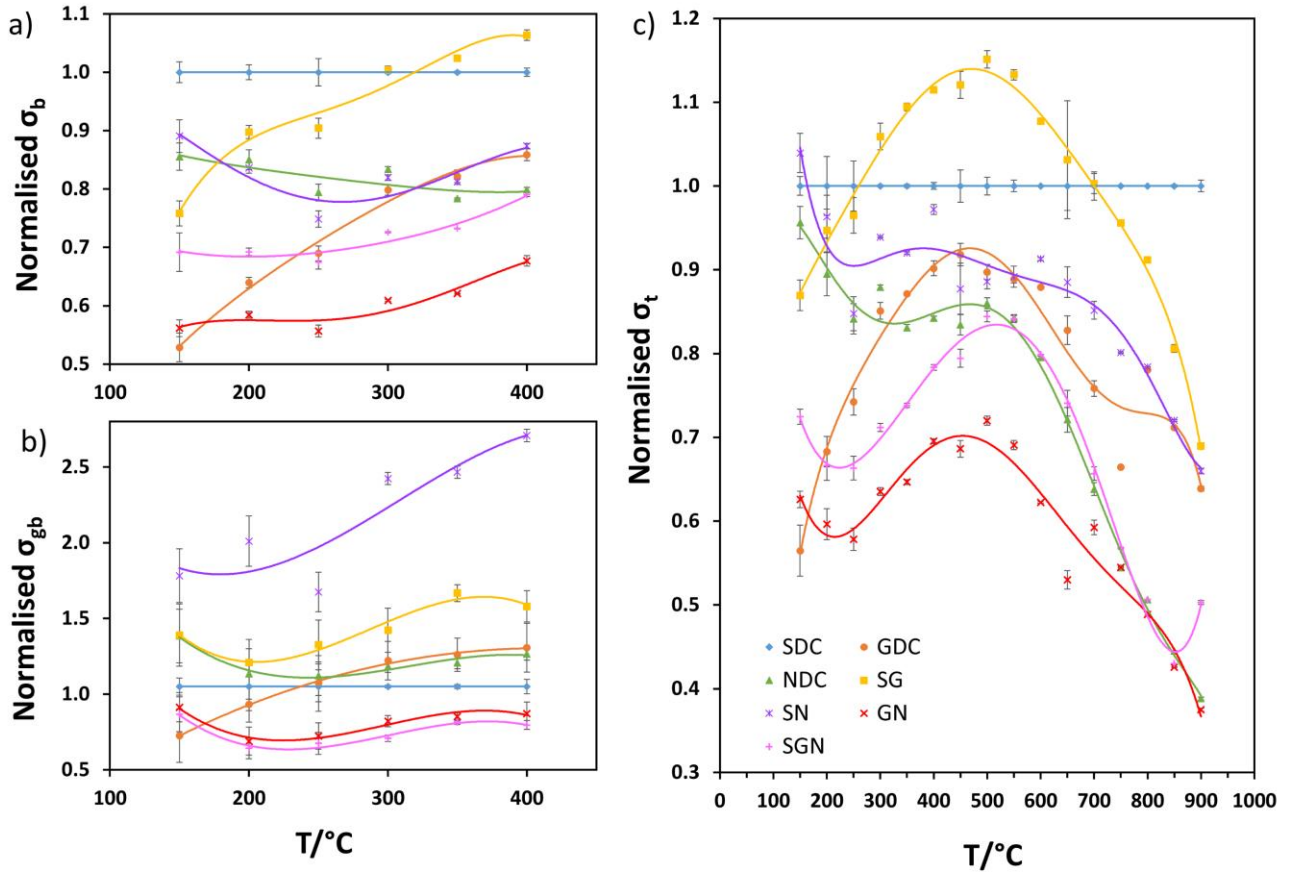
Figure 8. Plots of normalised (with respect to SDC) (a) bulk, (b) grain boundary and (c) total conductivity against measurement temperature for all samples.

lower grain boundary conductivities and these are linked to variations in preparation method and thus very probably to higher impurity levels, especially of Si, in the cited studies. Van Herle and co-workers obtained total ionic conductivity values of $5 - 7$ S m^{-1} at 750 °C in air for $Ce_{0.2}M_{0.8}O_{1.9}$ (M=Gd, Sm or Y) electrolytes prepared by a co-precipitation method.[34] This is comparable to the values of 6.58 S m^{-1} (SDC) and 6.29 S m^{-1} (SG) obtained here at the same temperature although the value for GDC (4.42 S m^{-1}) lies slightly below this range. The authors attributed their excellent ionic conductivity values to their high relative densities of around 97 %.

In Figure 8(c), normalised total conductivity, σ_t, is plotted over the whole range of measurement temperature, from 150 to 900 °C. At both 150 and 400 °C, the samples are arranged in the same order of increasing normalised σ_t as they were for σ_b in Figure 8(a). This again indicates the relatively small effect of σ_{gb} on σ_t and therefore that σ_t is determined essentially by σ_b. GDC had the lowest total conductivity at 150 °C, whereas GN was the lowest between 200 °C and 700 °C and between 800 °C and 900 °C and NDC was lowest at 750 °C. The highest values of σ_t were for SN at 150 °C,

15

for SDC at 200 °C and 250 °C and between 750 °C and 900 °C and for SG between 300 °C and 700 °C. The fact that SG has a higher conductivity than SDC − a widely used SOFC electrolyte composition − over this wide range of temperatures is technologically important given the drive to reduce SOFC operating temperatures and to develop IT-SOFCs for use between 500 and 700 °C. These results imply that SG would be a better electrolyte than SDC (or GDC) for such devices. For this reason, the Sm-Gd system is the subject of an ongoing detailed study by the present authors.

The combination of 10 mol % each of Sm^{3+} and Gd^{3+} is optimal for a 20 mol % doped ceria electrolyte at intermediate temperatures. This may be due to this specific combination of ionic radii giving increased oxygen ion mobility at these temperatures due to an optimal balance between migration and association enthalpies (see later). This could arise from the way the equal mix of Sm^{3+} and Gd^{3+} dopant ions forms defect clusters and complexes and the kind of structures that form.

The samples containing Nd (including GN) show a peak at very low temperatures in Figure 8(c) while those containing Gd (except GN) instead exhibit a sharp increase in normalised σ_t as temperature increased from its lowest value. This is a consequence of the increasing strengths of temperature dependence for Nd- < Sm- < Gd- containing samples which are reflected in the activation energies (see next section).

An important question in the field of SOFC electrolyte materials is whether co-doping results in detrimental, average or beneficial changes in conductivity with respect to the singly-doped, 'parent' materials. From Figure 8, the conductivity of SG is significantly higher than the singly-doped compounds, SDC and GDC, between 300 °C and 700 °C (the upper end of which are feasible IT-SOFC working temperatures). The greatest enhancement is observed at 500 °C where σ_t for SG is 15 % higher than that for SDC and 28 % higher than that for GDC. However, at the low and high extremes of the temperature scale, at 150 - 250 °C and 750 - 900 °C, σ_t for SG is intermediate between those of GDC and SDC. SN has σ_t values intermediate between those of SDC and NDC between 200 °C and 900 °C indicating an averaging effect. However, normalised σ_t for SN increases as temperature falls and is higher than for SDC or NDC (or any other sample) at 150 °C. Co-doping to form GN has a clearly detrimental effect since σ_t is lower than either GDC or NDC from 200 to 700 °C and only roughly equal to the lower of these at 150 °C (GDC) and 800 to 900 °C (NDC). The behaviour of the triply-doped sample (SGN) is similar. Again, its σ_t is lower than any of the three singly-doped materials at 250-500 °C but has similar values to the lowest of the three at 150 °C (GDC) and at 550-900 °C (NDC). Triple doping in this case is clearly detrimental. Taken overall, these results suggest that the conductivity of multiply-doped cerias

cannot always be interpreted simply as an average of the conductivities of the singly-doped parent materials, as was concluded in the computational study of Burbano *et al*.[22]

Dikmen and co-workers also reported that co-doping can improve the electrical performance of ceria-based electrolytes.[35][36] The ionic conductivity of $Ce_{0.8}Sm_{0.18}Gd_{0.02}O_{1.9}$ (2.88 S m^{-1}) was found to be almost twice as high as that for singly-doped $Ce_{0.8}Gd_{0.2}O_{1.9}$ (1.51 S m^{-1}), at 700 °C.[35] In the present study a similar enhancement was seen. Total conductivities at the same temperature were 4.40 S m^{-1} for SG ($Ce_{0.8}Sm_{0.1}Gd_{0.1}O_{1.9}$) and 3.30 S m^{-1} for GDC. The fact that these values are higher can be attributed to the different synthesis methods (citrate complexation compared to hydrothermal) and the different Sm:Gd ratios in the co-doped samples. However, a further study by Dikmen gave a maximum conductivity value of 6.50 S m^{-1} for $Ce_{0.8}Sm_{0.1}Gd_{0.1}O_{1.9}$ at 700 °C, which is approximately 50 % higher than the value obtained here for the same composition and temperature.[36]

Kahlaoui and co-workers found that the total conductivity of the co-doped material, $Ce_{0.8}Sm_{0.1}Nd_{0.1}O_{1.9}$, was higher - 3.29 S m^{-1} - than that of the singly-doped $Ce_{0.8}Sm_{0.2}O_{1.9}$ - 2.32 S m^{-1} – at 700 °C, both samples having been made by the citric acid-nitrate process.[37] In the present study, however, SN was found to have a lower total conductivity than SDC apart from at low temperatures (see Figure 8), although the absolute values at 700 °C were much higher for SDC - 4.39 S m^{-1} - and slightly higher for SN – 3.73 S m^{-1} - than those of Kahlaoui *et al*.[37] Thus, the higher conductivity of $Ce_{0.8}Sm_{0.1}Nd_{0.1}O_{1.9}$ synthesised by Kahlaoui *et al* compared to SDC may be due to an unusually low value for SDC.[37]

The highest total conductivity at 550 °C observed by Anirban and co-workers for the series of materials, $Ce_{0.9}Gd_{0.1-x}Nd_xO_{1.95}$ (0 ≤ x ≤ 0.1) prepared by citrate-nitrate auto-ignition, was 6.82 x 10^{-3} S m^{-1} when *x* = 0.075, which is significantly lower than the value of 0.635 S m^{-1} obtained here for the co-doped sample, GN, at the same temperature.[20] This is likely to be due to both the difference in dopant ratios (although they also report a value of 1.96 x 10^{-3} S m^{-1} at 550 °C for *x* = 0.05) and the difference in total dopant concentration: 10 % used by these authors and 20 % in the current study.[20]
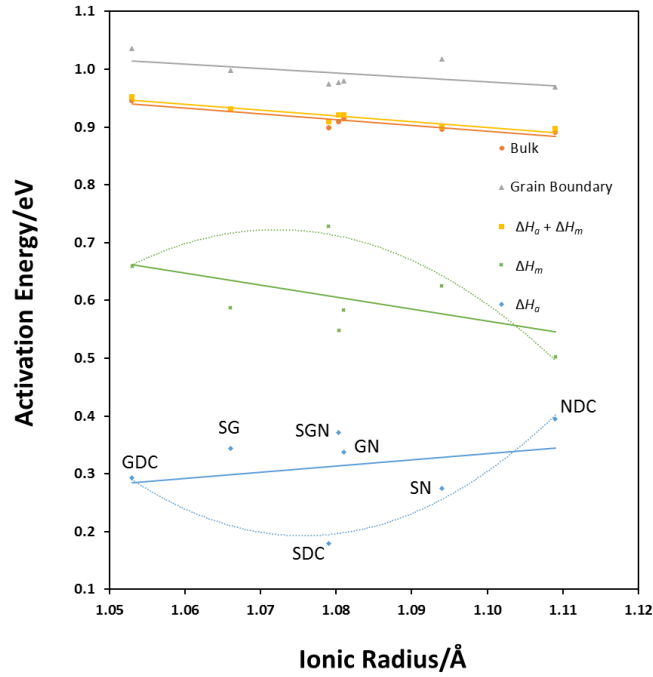
3.3.2 Activation Energies

Figure 9. Activation energies for bulk and grain boundary processes and total conductivity below (ΔH_m + ΔH_a) and above (ΔH_m) 450 °C and ΔH_a. The best fit lines are added as guides to the eye. See text for details.

In Figures 6 and S2, the plots of total conductivity contain a change in gradient at around 500 °C. This is a general and well-known effect for ionically-conducting aliovalently-doped ceramics which was explained by Steele for GDC.[38] At low temperatures, below this inflection point, defect clusters of the type $V_O^{\cdot\cdot} - M_{Ce}'$ (and some $M_{Ce}' - V_O^{\cdot\cdot} - M_{Ce}'$), are expected to be common, especially at high dopant concentrations like the 20 mol % value used here. These defect clusters dissociate progressively as temperature rises and above the inflection point it is assumed that no defect clusters remain, having all been thermally dissociated.. Therefore, at high temperatures, above the inflection point, we assume that the defect cluster concentration is insignificant and the gradient here can be equated to the migration enthalpy of the oxygen vacancies, ΔH_m, alone whilst below the inflection – where defect clusters are common and trap oxygen vacancies - it is equal to migration enthalpy plus the defect association enthalpy, $\Delta H_m + \Delta H_a$. Thus, by obtaining gradients above and below the inflection point, values for ΔH_m and ΔH_a can be calculated. Values of ΔH_m, ΔH_a, $E_t = \Delta H_m + \Delta H_a$ (from the low temperature section of the σₜ plot) as well as activation energies for bulk and grain boundary conductivity were calculated. These are plotted as a function of average dopant ionic radius in Figure 9 and compared to literature values in Table 3. Values for the pre-exponential constant were obtained by extrapolating the low temperature branch of the Arrhenius plots to the y-axis and these are presented in Figure 10.
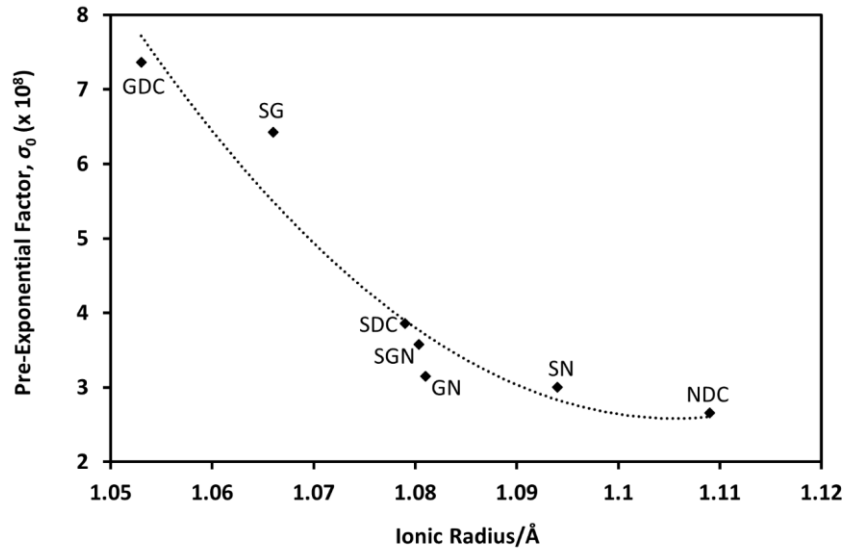
Figure 10. Variation of Pre-exponential constant, σ_o, with average ionic radius. The best fit line is added as a guide to the eye. See text for details.

The general trend for the activation energies for the bulk, grain boundary and total (below 500 °C, E_t) conductivities is a close-to-linear, gradual decrease with increasing average dopant ionic radius. The pre-exponential constant shows a decrease with increasing average ionic radius. The value for SG appears to be slightly higher than this general trend (the best-fit line) – which would act to increase conductivity - while the values for SGN and GN are slightly below it. Activation energy values for total and bulk conductivity are very similar, while those for grain boundary conductivity are considerably higher. The activation energies for SDC are very close to those reported by Konsinski and Baker for $Ce_{0.8}Sm_{0.2}O_{1.9}$ sintered under slightly different regimes.[24] The value of E_t for SDC (0.91 eV) is close to that reported by Balazs (0.85 eV) for the same composition.[32] Omar *et al* also found E_t values decreased in singly doped ceria with increasing dopant radius to an approximate minimum for the Nd-doped material.[18]

The values of ΔH_m and ΔH_a show more scatter than those of E_t in which they are combined. It is interesting to compare these plots with the work of Andersson *et al* who calculated values of ΔH_a and ΔH_m for ceria doped with lanthanides of atomic number, Z=57 (La) to 68 (Er).[14] Values for ΔH_a were obtained for two limiting cases in which dopant ions, M'_{Ce}, were (i) nearest neighbours (NN) or (ii) distant from each other (i.e. non-interacting). In each case, the electrostatic attraction (electronic interaction) and the lattice-mediated repulsion (elastic interaction) between the M'_{Ce} and $V_O^{\cdot\cdot}$ species were calculated and summed. This was done for vacancies in NN and next-nearest neighbour (NNN) sites, relative to the dopant ions. For both limiting cases, (i) and (ii), the overall interaction energy favoured the

NNN vacancy for lower Z (larger ions) and the NN position for the higher Z (smaller ions) with an energy minimum and cross-over between NN and NNN at 61 (Pm) for case (i) and 62 (Sm) for case (ii). The authors calculated a weighted average of the two cases corresponding to a dopant concentration of 4.2%, added a constant value for bulk ΔH_m (~0.5 eV) and obtained a valley-shaped dependence on atomic number with an energy minimum at Z=61/62. The ΔH_a values were about 0.18, 0. 16, 0,16 and 0.21 for Nd, Pm (and Nd:Sm in a 1:1 ratio), Sm and Gd doping, respectively. At the higher doping level of 20% used in the present work these values would be expected to be higher – because of the larger contribution from dopants in the case (ii) configuration - but still be in a similar valley-like relationship. In Figure 9, the ΔH_a values of the corresponding compositions – GDC, SDC, SN and NDC – do seem to form such a dependence (see construction line). However, SG, GN and SGN do not, but have ΔH_a values similar to, or slightly higher than, those for GDC.

Turning now to the migration enthalpy, ΔH_m, in the calculations just described, values were broadly similar to those found by Omar *et al*.[18] Andersson *et al* applied a constant value of ΔH_m which corresponded to vacancy migration distant from any dopant vacancies because of the low dopant concentration – 4.6% - that they considered. However, for a concentration of 20%, migration will more frequently be close to dopant sites and the influence of these on migration enthalpy should be included. Fortunately, these authors considered the energetics of migrations between the different oxygen sites in the vicinity of dopant sites. Considering the NN and NNN sites for the vacancy, they again found a cross-over in the lowest enthalpy of migration as a function of atomic number at around Z=62. However, this time the relationship was a volcano curve with – near the centre - values of ΔH_m of about 0.38, 0.40, 0.39, 0.33 eV for doping with Nd, Pm, Sm and Gd, respectively. This should be treated with some caution as it was calculated for the dopant ions NN to each other only and also the present authors have not included other vacancy migrations of higher energy which are likely also to make some contribution. However, the values of ΔH_m for these same dopants – NDC, SDC, SN, GDC – in Figure 9 do show a volcano-type relationship with a maximum around SDC. As was seen for ΔH_a, though, SG, GN and SGN do not fall on this curve (construction line).

Returning to the behaviour of the multiply doped samples in the present work, ΔH_a and ΔH_m values for GN and SN are averages of the values for their respective singly-doped parent compositions. Whereas Andersson *et al* used single (averaged) values of Z and of ionic radius for doubly-doped compositions, the computational work of Minervini *et al* and Burbano *et al* indicated that different co-dopants tend to retain their local coordination environment in the ceria

lattice.[14][11][22] Burbano *et al* presented calculations for double doping in two combinations of a small and a large dopant ion, Sc-La and Sm-Nd. They concluded that these doubly-doped materials had conductivities and activation energies that were an average of those of the parent, singly-doped compositions. This may be the case in the present work for both ΔH_m and ΔH_a of SN and GN (note that SN fits both the averaging and the Andersson *et al* model). However, where Sm and Gd are present together - in SG and SGN - the activation energies do not fit this model. Perhaps two such small dopant ions disrupt each other's local environment via the host lattice more strongly – competing for oxygen vacancies, for example - than a large and a small ion - whose coordination environments may be more complementary - especially at the relatively high dopant concentration used here (20%).

Table 3 compares literature values for ΔH_m and ΔH_a with those obtained here. Omar and co-workers obtained an approximately constant value for ΔH_a ~ 0.05 eV for $Ce_{1-x}Sm_{x/2}Nd_{x/2}O_{2-\delta}$ ($x = 0.08 - 0.18$) and a ΔH_m of 0.80 eV for $x = 0.18$, the highest value of x used, which differ considerably from the respective values obtained here of 0.28 and 0.63 eV for SN.[16] These differences may have arisen from the different synthesis procedures used: citrate complexation *vs.* conventional solid state.[16] Kilner gave experimental and calculated values for ΔH_a of GDC of 0.13 and 0.17 eV, respectively.[8] The former agrees with that for GDC given by Steele.[38] These values are lower than those acquired here but the calculated value is closest to that for SDC. The computational calculations of Minervini and co-workers gave ΔH_a for GDC of 0.38 eV (a little higher than the 0.29 eV obtained here).[11] Faber and co-workers obtained ΔH_a values by extrapolating their data to infinite dopant dilution, with the assumption that ΔH_m was 0.5 eV.[39] The average ΔH_m obtained here is 0.60 eV, which is in line with general values given by Kilner and Steele (0.6 eV) and Hohnke (0.61 eV). [40][41] For Nd and Gd dopants, this gave ΔH_a values of 0.23 and 0.32 eV, respectively, which compare with values of 0.40 and 0.29 eV acquired here for NDC and GDC, respectively, with 20% doping.

Poorly conducting grain boundaries would strongly affect total conductivity values, causing inaccuracies in the migration and association enthalpies acquired from them. However, this is not expected to be the case in this work as σ_{gb} was much higher than σ_b. This is the result of using the solution-based nitrate-citrate synthesis method, which aids in decreasing impurity levels. This method is also expected to promote atomic mixing of the host (Ce) and dopant (Sm, Gd, Nd) cations whereas the ceramic method may lead to the production of nanodomains with different dopant concentrations due to its reliance on inter-diffusion of the starting oxides.

4. Conclusions

A citrate complexation process was used to prepare a series of $Ce_{0.8}Sm_xGd_yNd_zO_{1.9}$ (x+y+z=0.2) nanopowders. Three singly-doped, $Ce_{0.8}M_{0.2}O_{1.9}$ (M=Sm, Gd, Nd), three doubly-doped, $Ce_{0.8}M_{0.1}M'_{0.1}O_{1.9}$ (M ≠ M'=Sm, Gd, Nd), and one triply-doped, $Ce_{0.8}Sm_{0.067}Gd_{0.067}Nd_{0.067}O_{1.9}$, materials were prepared. These – and dense sintered pellets made from them - were used in a detailed study of the effect of multiple doping on microstructure and ionic conductivity with the central aim to investigate the effect of the chemical composition on electrical properties.

The nanopowders had crystallite sizes of 55 to 93 Å and were high-purity, single-phase cubic fluorite materials which adhered to Vegard's Law. In the dense pellets, a general decrease in relative density with increasing average ionic radius of the dopant ion was observed. Average grain sizes showed no correlation with relative density or the average dopant ionic radius.

Impedance spectroscopy was carried out on the dense pellets. Grain boundary conductivity was much higher than bulk conductivity for all samples. This was linked to the low impurity contents achievable using the nitrate-citrate preparative method. Total conductivities of the singly-doped samples compared favourably with literature values.

Multiple doping was found to be detrimental (GN, SGN), averaging (SN) or beneficial (SG) compared to the singly-doped parent materials, depending on the combination of dopants present. There was some variation in these trends with temperature. These variations are attributed to the interplay between the activation energies of defect cluster association (ΔH_a) and oxygen ion migration ((ΔH_m), and the pre-exponential factor.

SG had significantly higher total conductivity than GDC, SDC or any other sample at 300-700 °C, having a value of 1.80 S m^{-1} at 600 °C. This indicates that SG should be of considerable interest for application as an electrolyte in IT-SOFCs. The Sm-Gd system is the subject of an ongoing study.

Although no conductivity enhancing effect was observed for the triply doped compound (SGN) relative to the three singly doped parent compounds, to the best of the authors' knowledge this is the first time conductivity data for this combination of dopants has been reported.

Arrhenius-type plots of conductivity were used to obtain association and migration enthalpies and these had respective values of between 0.18 (SDC) and 0.40 eV (NDC) and between 0.50 (NDC) and 0.73 eV (SDC). The trends in these enthalpies were discussed with reference to current models of doped cerias. For both association and migration enthalpies, connections to the computational model of Andersson *et al* is suggested for the singly-doped materials

(and possibly SN), while for GN (and possibly SN) these appeared to be averages of the values for the corresponding singly-doped parent materials. This demonstrates the effect of ceria electrolyte chemical composition on electrical properties. Lastly, the values for the samples containing Sm and Gd together showed a further behaviour which was tentatively related to the small size of both ions and the possibility that they may disrupt each other's local environment in the host lattice more than a combination of a small and a large dopant ion, especially at the relatively high dopant concentration (20%) used here.

5. Acknowledgements

References

[1] Y. Guo, M. Bessaa, S. Aguado, M.C. Steil, D. Rembelski, M. Rieu, J.-P. Viricelle, N. Benameur, C. Guizard, C. Tardivat, P. Vernoux, D. Farrusseng, An all porous solid oxide fuel cell (SOFC): a bridging technology between dual and single chamber SOFCs, Energy Environ. Sci. 6 (2013) 2119–2123.

[2] E.D. Wachsman, C.A. Marlowe, K.T. Lee, Role of solid oxide fuel cells in a balanced energy strategy, Energy Environ. Sci. 5 (2012) 5498–5509.

[3] H. Qin, Z. Zhu, Q. Liu, Y. Jing, R. Raza, S. Imran, M. Singh, G. Abbas, B. Zhu, Direct biofuel low-temperature solid oxide fuel cells, Energy Environ. Sci. 4 (2011) 1273–1276.

[4] J.C. Ruiz-Morales, D. Marrero-López, M. Gálvez-Sánchez, J. Canales-Vázquez, C. Savaniu, S.N. Savvin, Engineering of materials for solid oxide fuel cells and other energy and environmental applications, Energy Environ. Sci. 3 (2010) 1670–1681.

[5] A.B. Stambouli, E. Traversa, Solid oxide fuel cells (SOFCs): a review of an environmentally clean and efficient source of energy, Renew. Sustain. Energy Rev. 6 (2002) 433–455.

[6] T. Ishii, Y. Tajima, Low Temperature Operation of Solid Oxide Fuel Cell with a ZrO_2-Sc_2O_3-Al_2O_3 System Electrolyte, J. Electrochem. Soc. 141 (1994) 3450–3453.

[7] Y. Mishima, H. Mitsuyasu, M. Ohtaki, K. Eguchi, Solid oxide fuel cell with composite electrolyte consisting of samaria-doped ceria and yttria-stabilised zirconia, J. Electrochem. Soc. 145 (1998) 1004–1007.

[8]   J. Kilner, Fast oxygen transport in acceptor doped oxides, Solid State Ionics. 129 (2000) 13–23.

[9]   H.L. Tuller, A.S. Nowick, Doped ceria as a solid oxide electrolyte, J. Electrochem. Soc. 122 (1975) 255–259.

[10]   H. Inaba, H. Tagawa, Ceria-based solid electrolytes, Solid State Ionics. 83 (1996) 1–16.

[11]   L. Minervini, M.O. Zacate, R.W. Grimes, Defect cluster formation in M_2O_3-doped CeO_2, Solid State Ionics. 116 (1999) 339–349.

[12]   R. Shannon, Revised effective ionic radii and systematic studies of interatomic distances in halides and chalcogenides, Acta Crystallogr. Sect. A. 32 (1976) 751–767.

[13]   M. Mogensen, D. Lybye, N. Bonanos, P. V. Hendriksen, F.W. Poulsen, Factors controlling the oxide ion conductivity of fluorite and perovskite structured oxides, Solid State Ionics. 174 (2004) 279–286.

[14]   D.A. Andersson, S.I. Simak, N. V. Skorodumova, I.A. Abrikosov, B. Johansson, Optimization of ionic conductivity in doped ceria., Proc. Natl. Acad. Sci. U. S. A. 103 (2006) 3518–3521.

[15]   I. Stephens, J. Kilner, Ionic conductivity of $Ce_{1-x}Nd_xO_{2-x/2}$, Solid State Ionics. 177 (2006) 669–676.

[16]   S. Omar, E. Wachsman, J. Nino, Higher conductivity Sm^{3+} and Nd^{3+} co-doped ceria-based electrolyte materials, Solid State Ionics. 178 (2008) 1890–1897.

[17]   S. Omar, E. Wachsman, J. Nino, A co-doping approach towards enhanced ionic conductivity in fluorite-based electrolytes, Solid State Ionics. 177 (2006) 3199–3203.

[18]   S. Omar, E.D. Wachsman, J.L. Jones, J.C. Nino, Crystal Structure-Ionic Conductivity Relationships in Doped Ceria Systems, J. Am. Ceram. Soc. 92 (2009) 2674–2681.

[19]   F.-Y. Wang, B.-Z. Wan, S. Cheng, Study on Gd^{3+} and Sm^{3+} co-doped ceria-based electrolytes, J. Solid State Electrochem. 9 (2004) 168–173.

[20]   S. Anirban, T. Paul, P.T. Das, T.K. Nath, A. Dutta, Microstructure and electrical relaxation studies of chemically derived Gd–Nd co-doped nanocrystalline ceria electrolytes, Solid State Ionics. 270 (2015) 73–83.

[21]   Y. Liu, B. Li, X. Wei, W. Pan, Citric-nitrate combustion synthesis and electrical conductivity of the Sm^{3+} and Nd^{3+} co-doped ceria electrolyte, J. Am. Ceram. Soc. 91 (2008) 3926–3930.

[22]   M. Burbano, S. Nadin, D. Marrocchelli, M. Salanne, G.W. Watson, Ceria co-doping: synergistic or average effect?, Phys. Chem. Chem. Phys. 16 (2014) 8320–8331.

[23]   R.O. Fuentes, R.T. Baker, Structural, morphological and electrical properties of $Gd_{0.1}Ce_{0.9}O_{1.95}$ prepared by a citrate complexation method, J. Power Sources. 186 (2009) 268–277.

[24]   M.R. Kosinski, R.T. Baker, Preparation and property–performance relationships in samarium-doped ceria nanopowders for solid oxide fuel cell electrolytes, J. Power Sources. 196 (2011) 2498–2512.

[25]   A.R. Denton, N.W. Ashcroft, Vegards law, Phys. Rev. A. 43 (1991) 3161–3164.

[26]   H. Klug, L. Alexander, X-Ray Diffraction Procedures for Polycrystalline and Amorphous Materials, John Wiley, New York, 1974.

[27]   T.H. Kwon, T. Lee, H.I. Yoo, Partial electronic conductivity and electrolytic domain of bilayer electrolyte $Zr_{0.84}Y_{0.16}O_{1.92}/Ce_{0.9}Gd_{0.1}O_{1.95}$, Solid State Ionics. 195 (2011) 25–35.

[28]   K.R. Lee, J.H. Lee, H.I. Yoo, Reassessment of conventional polarization technique to measure partial electronic conductivity of electrolytes, Solid State Ionics. 181 (2010) 724–729.

[29]   T. Shimonosono, Y. Hirata, Y. Ehira, S. Sameshima, T. Horita, H. Yokokawa, Electronic conductivity measurement of Sm- And La-doped ceria ceramics by Hebb-Wagner method, Solid State Ionics. 174 (2004) 27–33.

[30]   T. Shimonosono, Y. Hirata, S. Sameshima, T. Horita, Electronic conductivity of La-doped ceria ceramics, J. Am. Ceram. Soc. 88 (2005) 2114–2120.

[31]   J.T.S. Irvine, D.C. Sinclair, A.R. West, Electroceramics: characterization by impedance spectroscopy, Adv. Mater. 2 (1990) 132–138.

[32]   G.B. Balazs, R.S. Glass, ac impedance studies of rare earth oxide doped ceria, Solid State Ionics. 76 (1995) 155–162.

[33]   Z. Zhan, T.-L. Wen, H. Tu, Z.-Y. Lu, AC Impedance Investigation of Samarium-Doped Ceria, J. Electrochem. Soc. 148 (2001) A427–A432.

[34]   J. Van Herle, M. Dokiya, T. Horita, T. Kawada, N. Sakai, H. Yokokawa, Low temperature fabrication of (Y, Gd, Sm)-doped ceria electrolyte, Solid State Ionics. 86–88 (1996) 1255–1258.

[35]   S. Dikmen, H. Aslanbay, E. Dikmen, O. Şahin, Hydrothermal preparation and electrochemical properties of Gd^{3+} and Bi^{3+}, Sm^{3+}, La^{3+}, and Nd^{3+} codoped ceria-based electrolytes for intermediate temperature-solid oxide fuel cell, J. Power Sources. 195 (2010) 2488–2495.

[36]   S. Dikmen, Effect of co-doping with Sm^{3+}, Bi^{3+}, La^{3+}, and Nd^{3+} on the electrochemical properties of hydrothermally prepared gadolinium-doped ceria ceramics, J. Alloys Compd. 491 (2010) 106–112.

[37]   M. Kahlaoui, S. Chefi, A. Inoubli, A. Madani, C. Chefi, Synthesis and electrical properties of co-doping with

La^{3+}, Nd^{3+}, Y^{3+}, and Eu^{3+} citric acid-nitrate prepared samarium-doped ceria ceramics, Ceram. Int. 39 (2013) 3873–3879.

[38] B.C.H. Steele, Appraisal of Ce$_{1-y}$Gd$_y$O$_{2-y/2}$ electrolytes for IT-SOFC operation at 500 °C, Solid State Ionics. 129 (2000) 95–110.

[39] J. Faber, C. Geoffroy, A. Roux, A. Sylvestre, P. Abelard, A systematic investigation of the dc-electrical conductivity of rare-earth-doped ceria, Appl. Phys. A. 49 (1989) 225–232.

[40] J.A. Kilner, B.C.H. Steele, Non-stoichiometric Oxides, Academic Press, New York, 1981.

[41] D.K. Hohnke, Ionic conduction in doped oxides with the fluorite structure, Solid State Ionics. 5 (1981) 531–534.

[42] D. Pérez-Coll, P. Núñez, J.R. Frade, Improved conductivity of Ce$_{[1-x]}$Sm$_{[x]}$O$_{[2-\delta]}$ ceramics with submicrometer grain sizes, J. Electrochem. Soc. 153 (2006) A478–A483.

[43] S. Ramesh, V.P. Kumar, P. Kistaiah, C.V. Reddy, Preparation, characterization and thermo electrical properties of co-doped Ce$_{0.8-x}$Sm$_{0.2}$Ca$_x$O$_{2-\delta}$ materials, Solid State Ionics. 181 (2010) 86–91.

[44] X. Sha, Z. Lü, X. Huang, J. Miao, L. Jia, X. Xin, W. Su, Preparation and properties of rare earth co-doped Ce$_{0.8}$Sm$_{0.2-x}$Y$_x$O$_{1.9}$ electrolyte materials for SOFC, J. Alloys Compd. 424 (2006) 315–321.

[45] D. Perez-Coll, D. Marrero-Lopez, P. Nunez, S. Pinol, J.R. Frade, Grain boundary conductivity of Ce$_{0.8}$Ln$_{0.2}$O$_{2-\delta}$ ceramics (Ln = Y, La, Gd, Sm) with and without co-doping, Electrochim. Acta. 51 (2006) 6463–6469.

[46] Y.P. Fu, S.H. Chen, J.J. Huang, Preparation and characterization of Ce$_{0.8}$M$_{0.2}$O$_{2-\delta}$ (M = Y, Gd, Sm, Nd, La) solid electrolyte materials for solid oxide fuel cells, Int. J. Hydrogen Energy. 35 (2010) 745–752.

Tables

Table 1. Lattice parameters, a, unit cell volumes, V and crystallite sizes as calculated by the Scherrer equation from powder XRD data, D_{XRD} and as measured from TEM images, D_{TEM}, for $Ce_{0.8}Sm_xGd_yNd_zO_{1.9}$ powders calcined at 500 °C for 2 h.

Formula	Notation	a/Å	V/Å^3	D_{XRD}/Å	D_{TEM}/Å
$Ce_{0.8}Sm_{0.2}O_{1.9}$	SDC	5.4323 ± 0.0002	160.31 ± 0.02	67 ± 1.0	75 ± 18
$Ce_{0.8}Gd_{0.2}O_{1.9}$	GDC	5.4244 ± 0.0001	159.61 ± 0.01	93 ± 2.0	109 ± 32
$Ce_{0.8}Nd_{0.2}O_{1.9}$	NDC	5.4446 ± 0.0004	161.40 ± 0.04	55 ± 0.5	81 ± 37
$Ce_{0.8}Sm_{0.1}Gd_{0.1}O_{1.9}$	SG	5.4279 ± 0.0002	159.92 ± 0.02	77 ± 1.5	95 ± 25
$Ce_{0.8}Sm_{0.1}Nd_{0.1}O_{1.9}$	SN	5.4410 ± 0.0006	161.08 ± 0.05	69 ± 1.0	83 ± 8
$Ce_{0.8}Gd_{0.1}Nd_{0.1}O_{1.9}$	GN	5.4352 ± 0.0003	160.56 ± 0.03	72 ± 1.0	95 ± 23
$Ce_{0.8}Sm_{0.2/3}Gd_{0.2/3}Nd_{0.2/3}O_{1.9}$	SGN	5.4342 ± 0.0003	160.48 ± 0.03	63 ± 1.0	89 ± 21

Table 2. Concentrations of cations as determined by ICP-MS for all powder samples. Errors are ± one standard deviation.

Sample	Ce (cation %)	Sm (cation %)	Gd (cation %)	Nd (cation %)
SDC	78.3 ± 2.0	20.9 ± 0.5	0.70 ± 0.02	0.045 ± 0.001
GDC	77.1 ± 5.1	0.074 ± 0.005	22.8 ± 1.5	0.0132 ± 0.0009
NDC	77.7 ± 7.5	0.016 ± 0.002	0.75 ± 0.07	21.6 ± 2.1
SG	77.8 ± 3.0	10.5 ± 0.4	11.7 ± 0.5	0.027 ± 0.001
SN	78.3 ± 1.2	10.7 ± 0.2	0.67 ± 0.01	10.3 ± 0.2
GN	78.6 ± 5.4	0.021 ± 0.001	11.4 ± 0.8	10.0 ± 0.7
SGN	78.4 ± 1.3	6.9 ± 0.1	7.9 ± 0.1	6.7 ± 0.1

Sample	Ce (cation %)	Sm (cation %)	Gd (cation %)	Nd (cation %)

Table 3: Comparison of the activation energy and association and migration enthalpy values obtained in this study with those reported in the literature for equivalent samples where possible. Where the literature composition is known and is different from that of this study, it is indicated.

Sample	Activation Energy/eV						Migration Enthalpy/ eV	Migration Enthalpy (literature)/eV	Association Enthalpy/eV	Association Enthalpy (literature)/eV
	Bulk	Bulk (literature)	Grain Boundary	Grain Boundary (literature)	Total (≤ 450 °C)	Total (literature)				
SDC	0.90	0.85 [42]	0.98	0.94 [43]	0.91	0.85 [32]	0.73	0.69 [44]	0.18	0.26 [42]
GDC	0.95	0.94 [45]	1.04	-	0.95	0.75 [46]	0.66	-	0.29	0.17 (calculated) and 0.13 (experimental) [8], 0.13 ($Ce_{0.9}Sm_{0.1}O_{1.95}$) [38], 0.32 (composition unknown) [39], 0.38 (composition unknown) [11]
NDC	0.89	-	0.97	-	0.90	0.78 [32]	0.50	-	0.40	0.23 (composition unknown) [39]
SG	0.93	-	1.00	-	0.93	0.59 [36]	0.59	-	0.34	-
SN	0.90	0.93 [37]	1.02	0.90 [37]	0.90	0.92 [37]	0.63	0.80 ($Ce_{0.82}Sm_{0.09}Nd_{0.09}O_{2-\delta}$) [16]	0.28	~0.05 ($Ce_{0.82}Sm_{0.09}Nd_{0.09}O_{2-\delta}$) [16]
GN	0.92	-	0.98	-	0.92	0.98 ($Ce_{0.9}Gd_{0.05}Nd_{0.05}O_{1.95}$) [20]	0.58	-	0.34	-
SGN	0.91	-	0.98	-	0.92	-	0.55	-	0.37	-

Figure Captions

Figure 1. XRD patterns for powder samples of $Ce_{0.8}Sm_xGd_yNd_zO_{1.9}$ for all compositions. *Small peak at about 45° is due to the sample holder (main peak of Fe).

Figure 2. Dependence on average ionic radius of dopant ions in $Ce_{0.8}Sm_xGd_yNd_zO_{1.9}$ of a) lattice parameter obtained from powder XRD; b) average crystallite size calculated from powder XRD data and TEM images; c) relative density of pellets sintered at 1450°C for 4h. The best fit lines are added as guides to the eye.

Figure 3. SEM images at intermediate and high magnification alongside log histograms showing the grain area distributions for samples sintered at 1450°C for 4h: a) SDC, b) GDC, c) NDC, d), SG, e) SN, f) GN and g) SGN..

Figure 4. Average grain diameter (calculated from grain areas with the assumption that grain cross-sections are circular) as a function of average ionic radius of dopant ions for $Ce_{0.8}Sm_xGd_yNd_zO_{1.9}$ samples sintered at 1450°C for 4 h. The best fit line is added as a guide to the eye.

Figure 5. Nyquist plots for SDC, GDC, NDC, SG, SN, GN and SGN at a) 250°C, b) 500°C and c) 750°C. Different symbols represent the change in frequency decade, the key for which is inset in panel (c).

Figure 6. Arrhenius plots of total (♦), bulk (●) and grain boundary (▲) conductivity for SG.

Figure 7. Log plots of (a) total, (b) bulk and (c) grain boundary conductivity against average ionic radius for all samples.

Figure 8. Plots of normalised (with respect to SDC) (a) bulk, (b) grain boundary and (c) total conductivity against measurement temperature for all samples.

Figure 9. Activation energies for bulk and grain boundary processes and total conductivity below ($\Delta H_m + \Delta H_a$) and above (ΔH_m) 450 °C and ΔH_a. The best fit lines are added as guides to the eye. See text for details.

Figure 10. Variation of Pre-exponential constant, $\boldsymbol{\sigma_o}$, with average ionic radius. The best fit line is added as a guide to the eye. See text for details.